Design & Development of a Galvanometer Inspired Dual Beam Optical Coherence Tomography System for Flow Velocity Quantification of the Microvasculature

S.M. Daly[1,*], E. Jonathan[1], M.J. Leahy[1,2]
[1]*Biophotonics Research Facility, Dept. of Physics & Energy, University of Limerick, Ireland*
[2]*Royal College of Surgeons (RCSI), Dublin, Ireland*

ABSTRACT

This paper reports initial experimentation of a dual beam flow velocity estimation setup based on optical coherence tomography (OCT) for biomedical applications. The proposed work incorporates a low cost switching mechanism (rotating galvanometer mirror) for optical signal discrimination between adjacent fiber channels enabling quasi-simultaneous multiple specimen scanning. A cascaded interferometric design is used with two sample output arms orientated in parallel to eachother. A cross-correlation computation between these two parallel sample beams yields a relative time delay, enabling assessment and quantification of flow velocities.

Keywords: Microcirculation, Dual Beam, Velocity, Optical Coherence Tomography, Cross-Correlation

1. INTRODUCTION

'Microcirculation' is a noun which defines the movement (in this instance, flow) of blood or lymph through the smallest conduits of the human vasculature network via the venules, arterioles and in particular, capillaries. The microcirculation serves several key functions within the body including regulation of blood pressure, flow and body temperature, delivery of nutrients and removal of metabolic waste products.

Often, diseases of early developmental origin can manifest themselves in the microcirculation long before a definitive clinical diagnosis is made. For example, in the nailfold plexus the capillaries come within 200μm of the surface of the skin, the fingernail is easily fixed in position and the capillaries run parallel to the skin surface. Structural and functional changes within the microcirculation have previously been associated with various pathological conditions and chronic illnesses such as scleroderma[1], systemic sclerosis[2], antiphospholipid syndrome[3], connective tissue disease[4], *diabetes mellitus*[5] and Raynaud's phenomenon[2] to name but a few, have been readily identified via specific physiological markers such as vessel permeability, the presence of avascular areas, enlarged loops and poor circulation. In addition, the identification of such ailments has not been limited to solely systemic diseases; localised areas of pain have manifested in the nailfold revealing conditions such as rheumatoid arthritis[6], vasculitis, psoriasis and psoriatic arthritis[7], and migraine, in addition to mental disorders such as schizophrenia[8]. More recently, however, the extent to which the microcirculation of the nailfold plexus represents that of other parts of the body has been questioned. Methods which would allow the routine clinical assessment and monitoring at the microcirculatory level could greatly improve early detection, and thus better recovery rates for patients.

The analysis of light interactions with tissue could perform a non-invasive 'optical biopsy'; this may play a crucial role wherein treatment progression depends on the pathologic result of biopsy. Due to the complexity of the biological environment, there is difficulty in obtaining accurate data when subject to enormous variability[9]. Furthermore, *ex vivo* tissue is not representative of the natural environment. Non-invasive imaging techniques have filled this niche, garnering a reputation for fulfilling patient comfort during clinical assessment.

* Corresponding author: susan.mcelligott@ul.ie

Optical Coherence Tomography and Coherence Techniques V, edited by Rainer A. Leitgeb, Brett E. Bouma, Proc. of SPIE-OSA Biomedical Optics, SPIE Vol. 8091, 809121

Minimally invasive imaging techniques have revolutionised diagnostic medicine. In the past two decades, advances in optics, fiber as well as laser technology have enabled the development of a novel non-invasive optical biomedical imaging technology[10], Optical Coherence Tomography (OCT). Partial (or low) coherence interferometry (PCI), a technique first applied to the biomedical field for measurement of the axial eye length[11], forms the fundamental tenets of OCT. PCI records optical A-scans of the measured object(s) and plots the back-reflected intensity as a function of depth position; it is analogous to conventional ultrasonic pulse-echo imaging and is in essence 'optical ultrasound'.

OCT is an established imaging technique which performs cross-sectional imaging in (biological) materials by measuring the magnitude of backscattered light from within a sample as a function of the optical delay time. With the development of Fourier-domain OCT, faster imaging has been achieved[12-14]. However, these high acquisition rates were inevitably of low sensitivity to flow rates, and although a commercial OCT system can scan at very rapid rates and perform velocity estimation, it is not capable of performing this simultaneously at two distinct points. In addition, biological processes are unpredictable in nature and the possibility that a biological effect of importance may have occurred during scanning intervals cannot be overlooked, especially when a diagnosis is being sought. This system has been constructed in an effort to alleviate this uncertainty in the most cost effective means as possible.

The advantages of the proposed system are 4-fold: (1) the use of a galvoscanning mirror reduces the requirements of having two separate spectrometers for spectral detection and thereby reduces overall cost; (2) the condition for interference is satisfied before the galvoscanning mirror, which serves as an efficient intermediary for transferring the separate light beams to the spectrograph; (3) crosstalk between the adjacent channels was avoided by mounting each sample beam focusing lens within a Teflon holder. Each lens was chosen to have a different effective focal length (EFL) and as such needed to be spatially displaced axially and adjusted to meet the condition for interference; (4) the use of a single mirror as a stationary reference for both beams also contributes to the overall cost-effectiveness of the system.

The potential of the aforementioned dual-beam configuration for simultaneous imaging at two spatially distinct positions as an alternative approach to achieving absolute values of velocity is explored in this proof of principle study.

2. THEORETICAL FRAMEWORK

2.1 Fourier domain OCT (Spectral domain, Sd-OCT)

Michelson interferometry is the basis of OCT. A monochromatic light source emits a source beam horizontally towards a diagonally inclined beamsplitter (BS), splitting the source beam in two. While one half is reflected off the BS and then backreflected by a reference mirror, the other half is transmitted through the BS and then backreflected by an object surface.

These two beams are then recombined by the beamsplitter and received by a detector. The two backreflected electric fields may be represented by phasor expressions (neglecting polarisation):

$$E_R = E_{R0} \exp(i(2k_R l_R - \omega t)) \tag{1}$$

$$E_S = E_{S0} \exp(i(2k_S l_S - \omega t)) \tag{2}$$

R and S denote the reference and sample arms respectively; E_{R0} and E_{S0} denote the electric field amplitudes of the beams; k_R and k_S denote propagation constants; l_R and l_S denote the two arm lengths measured from the BS; ω and t denote frequency and time respectively.

The electric field of the recombined beam is a superposition of the two monochromatic electric fields:

$$E = E_R + E_S \tag{3}$$

Backscatterers at various depths are considered, implying the sample beam consists of multiple partial waves emanating from the backscatterers. As before, the spectral components of the reference and sample beams are:

$$E_R(\omega) = E_0(\omega) r_R \exp(i(2k_R(\omega)l_R - \omega t)) \tag{4}$$

$$E_S(\omega) = E_0(\omega) \int_{-\infty}^{\infty} r_S'(l_S) \exp(i(2k_S(\omega)l_S - \omega t)) dl_S \tag{5}$$

where $E_0(\omega)$ denotes the electric field incident on the reference mirror or sample surface; r_R is the amplitude reflectivity of the reference mirror; $r_S'(l_S)$ is the apparent amplitude reflectivity density of the backscatterers along the A-line. If dispersion is neglected:

$$k = \frac{\omega}{c} \tag{6}$$

The resulting spectral interferogram is given by:

$$I(k) = \left| E_R(kc) + E_S(kc) \right|^2 \tag{7}$$

and substituting Eqs. 4 and 5 into Eq. 7 yields:

$$I(k) = \underbrace{S(k) r_R^2}_{reference-\text{intensity}} + \underbrace{2S(k) r_R \int_{-\infty}^{\infty} r_s'(l_s) \cos(2k(n_s l_s - l_R)) dl_s}_{cross-\text{interference}} + \underbrace{S(k) \left| \int_{-\infty}^{\infty} r_s'(l_s) \exp(i2k(n_s l_s)) dl_s \right|^2}_{self-\text{interference}} \tag{8}$$

The cross interference term can be decoded to extract $r_s'(l_s)$ by taking the inverse Fourier transformation. In order to recover the true image, measure the reference intensity term by blocking the sample arm ($r_s' = 0$), measure the self-interference term by blocking the reference arm ($r_R = 0$) and then subtract both of these terms from the right hand side of Eqn. 8.

2.2 Dual-beam Modality

Several investigations have reported the use of a dual-beam imaging modality. The classic interferometric setup of PCI and OCT has the drawback of being sensitive to longitudinal object positions. Efforts to overcome such limitations were outlined by Baumgartner *et al.*[15], in which a special common path dual-beam ocular interferometric set-up utilised the cornea as a reference surface, a diffractive optical element for wavefront matching and two spectrally displaced synthesised SLDs for improved axial resolution. The dual-beam modality was reported to be capable of providing useful information on the microstructure of the human ocular fundus and improving SNR. Bachmann *et al.*[16] also reported results pertaining to a similar type of OCT set-up; this dual-beam setup exploited the possibility of high phase stability between successive spectra through this common path configuration.

The aforementioned reported works used 'dual-beam' in the context of a common path configuration; other works (including this one) used 'dual beam' imaging to imply the use of two spatially separated light beams to illuminate a specimen at separate distinct points.

A dual beam Doppler Sd-OCT system was reported by Iftimia *et al*. which eliminated the ambiguity associated with unknown orientation of local velocity vectors in the blood vessels of zebrafish[17]. This Sd-OCT technique integrated two interferometers with coupled components and different sample/reference pathlengths to avoid crosstalk, enabling the

measurement of absolute velocity values. However, sensitivity to flow is inversely proportional to the acquisition speed. Hence, the flow sensitivity of Doppler Fd-OCT is low owing to the high acquisition rates[18]. Classical point-scanning confocal microscopy is too slow to record the motion of rapidly moving blood cells. In an effort to over come this limitation, scanning has been performed along a designated line either parallel or perpendicular to a vessel. The length of the cell trace divided by time reveals the velocity. This technique provides valuable hemodynamic measurements, although it is very time consuming[19].

A multiple beam approach is desired since the precise orientation of the vasculature is unknown *a priori*. Additionally, as the vasculature of primary interest lies in (approximately) a single plane (dermal layer), symmetry may be exploited reducing the number of beams required to two, irrespective of vessel tortuosity. To improve flow sensitivity, acquisition speeds have to be decreased (undesirable, especially at high velocities) or multiple scans should be obtained from the same sample position. In addition, the time difference could be augmented by increasing the beam separation; thus, flow sensitivity may be improved without reducing the scanning speed.

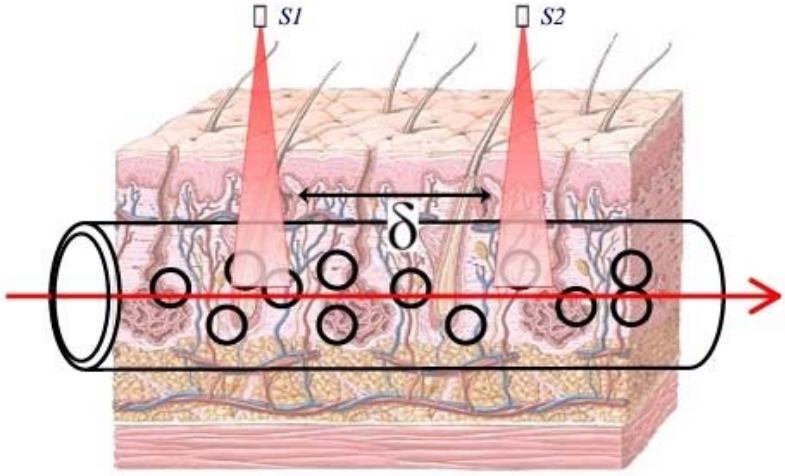

Figure 1. Illustration of the dual-beam modality within the vasculature. δ indicates the beam separation (measured *a priori*). (Not to scale.)

The mathematical expression for cross-correlation is given by the following:

$$(A * B)(t) = \int_{-\infty}^{\infty} A^*(\tau) B(t+\tau) d\tau \tag{9}$$

If two real valued functions **A** and **B** are considered, which differ only by an unknown shift along the x-axis, cross-correlation may be used to determine how much **B** must be shifted along the x-axis to make it identical to **A**. Cross-correlation is essentially a dot product operation which slides the **A** function along the x-axis, calculating the integral of their product at each position. When the functions match, a value of correlation is maximised.

By knowing the time difference between the adjacent frames and the number of frames between signals **A** and **B**, the time lag ($\Delta\tau$) can be calculated. Therefore, by obtaining the quotient the spatial separation of the two beams and the time lag, $\delta/\Delta\tau$, a value for the velocity may be computed. The method of cross-correlation has been used in the development of a robust algorithm for vehicle motion tracking for surveillance purposes[20].

3. EXPERIMENTAL DESIGN

3.1 Sd-OCT dual beam system design

Since its inception, the basic design of a fiber low-coherence interferometer has remained largely the same, with typical configurations featuring (2x2) couplers and single reference/sample arms[21]. However, for our purposes, a cascaded interferometric design was used and the sample output fibers were orientated parallel to eachother and approximately perpendicular with respect to the specimen under study.

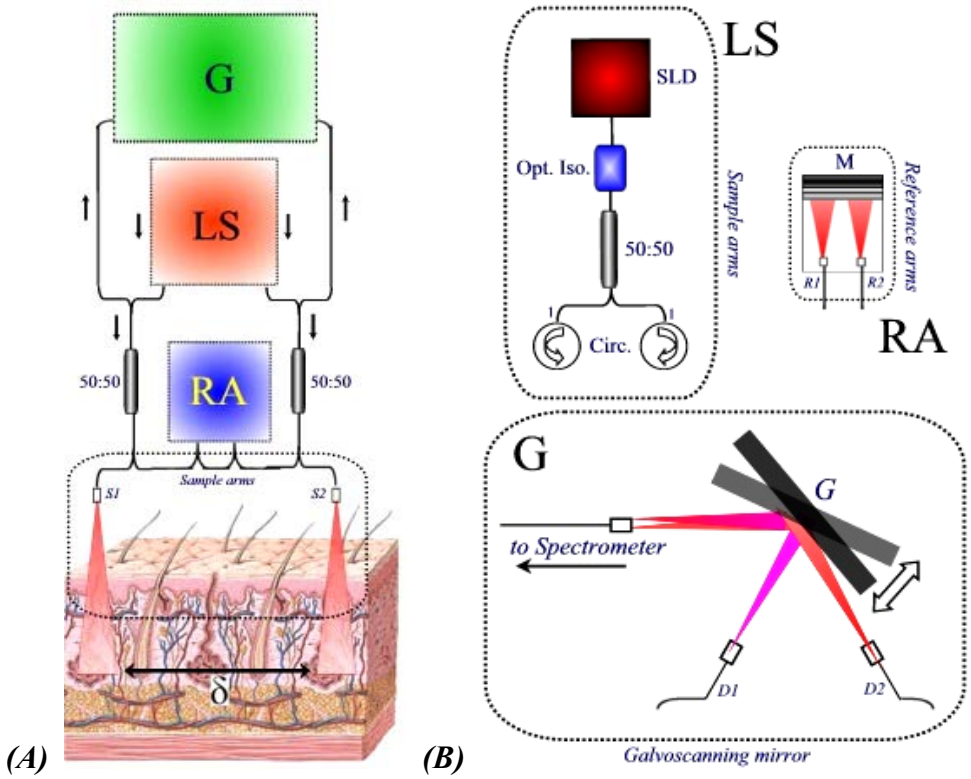

Figure 2. **(A)** Simplified schematic of dual beam Sd-OCT system. S1, S2 = focusing lenses. **(B)** Enlarged, detailed versions of (A). **LS** = light source; SLD = superluminescent diode, Opt. Iso. = optical isolator, x:y = splitting ratio of the fiber couplers (50%), Circ. = circulators. **RA** = reference arms; common mirror arrangement; R1, R2 = collimating lenses. **G** = galvoscanning mechanism; D1, D2 = collimating lenses.

The chosen light source is a broadband, superluminescent diode (Integrated box SLED, BX10 Series, Denselight, Singapore) with a full-width-half-maximum bandwidth of 130 nm at 3 dB centred at 1.31 μm. The light source yields a measured axial resolution of 5.83 μm in air. This light is coupled into an optical isolator, to a 50:50 beamsplitter and then subsequently split into its required amount of arms by using appropriate beamsplitters (50:50).

Fiber collimating lenses were used in the reference arms and focusing fiber lenses for both sample arms. To limit the amount of possible crosstalk between the sample beam channels, the sample arms were encased in Teflon material and aligned parallel to each other (see Fig. 3, below). Each focusing lens was chosen to have a different effective focal length (EFL), so stray light reflections would not induce fluctuations in either sample arm.

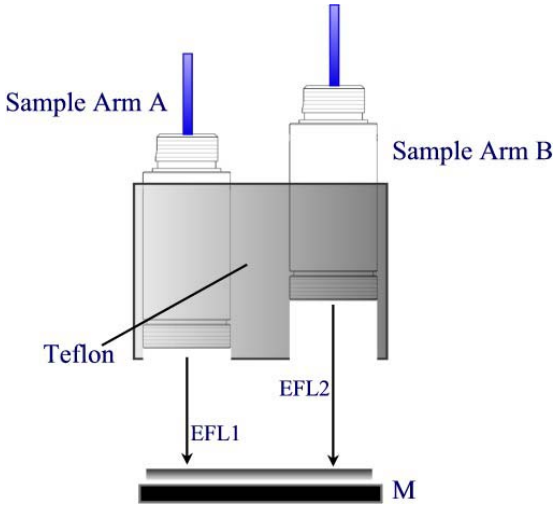

Figure 3. Illustration of the sample beam configuration for dual beam analysis. The two focusing lenses were encased in Teflon in order to eliminate possible channel crosstalk. As *EFL2* > *EFL1*, sample arm B needed to be displaced axially to enable simultaneous interference from both arms with their respective references. M = broadband dielectric mirror.

In order to perform alternate scanning of the two sample arms, a single galvoscanning arm (Thorlabs, GVS002) was used, which was connected to the PC via a connector block (SCC-68, National Instruments, USA) and a peripheral control interface card (PCI-6731, National Instruments, USA) The galvoscanning mechanism was operated via LabVIEW (Laboratory Virtual Instrumentation Engineering Workbench) software. Movement of the galvomirror was accomplished by inputting a sine wave to raster scan between the sample arms.

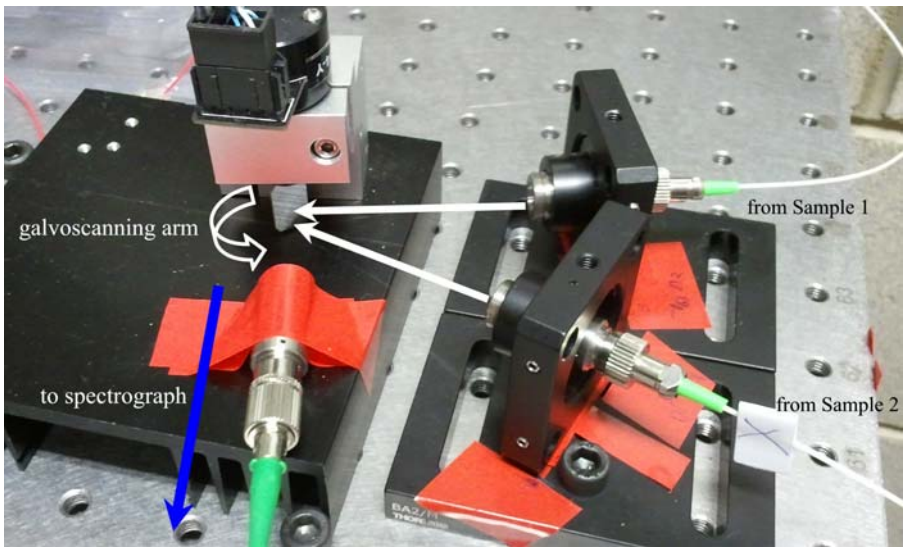

Figure 4. The experimental set-up used during dual beam scanning measurements. The two collimating lenses (right in picture) directed the light from the two focusing sample lenses to the galvoscanning mirror, which coupled the signal information to another collimating lens. This final lens relayed the alternating signals to the spectrograph.

The light reflected from the galvoscanning arm from each sample was coupled into a collimating lens connected to a makeshift patch chord (99:1 coupler) which served as the conduit, presenting each sample arm interference signal(s) in turn to the spectrograph (BaySpec, OCTS-1249-1310-1371) via a FC/APC connection (see Fig. 2(B)**G** and Fig. 4 above).

For the purposes of these experiments, the galvoscanning mirror was set to rotate at a frequency of 15 Hz and a camera exposure time of 0.0278 s was chosen.

Throughout the system, single mode fibers were utilised to ensure there was no broadening of the axial resolution. A 14-bit line scan camera (Goodrich SU-LDH Digital Line Scan Camera; 1024 pixels) was used with a maximum line scan rate of 46992 Hz. The camera was connected via a Camera Link terminal to a high-speed frame grabber board (PCIe-1427, National Instruments, USA).

3.2 Experimental procedure

The experimentation was implemented by initialising flow in a capillary tube (Ø = 0.8 mm (inner diameter); VitroCom). The liquid used was 1% dilution of 10% Intralipid™ solution used to emulate blood flow[22], as within the human vasculature. A commercial OCT system (Thorlabs, OCMP1300SS), using the Doppler setting, was used to determine an appropriate flow rate which would establish laminar flow within the capillary. A flow rate of 0.075 ml min^{-1} (1.97 mm s^{-1}) was chosen and implemented through the use of a syringe pump (Harvard Apparatus, PHD2000).

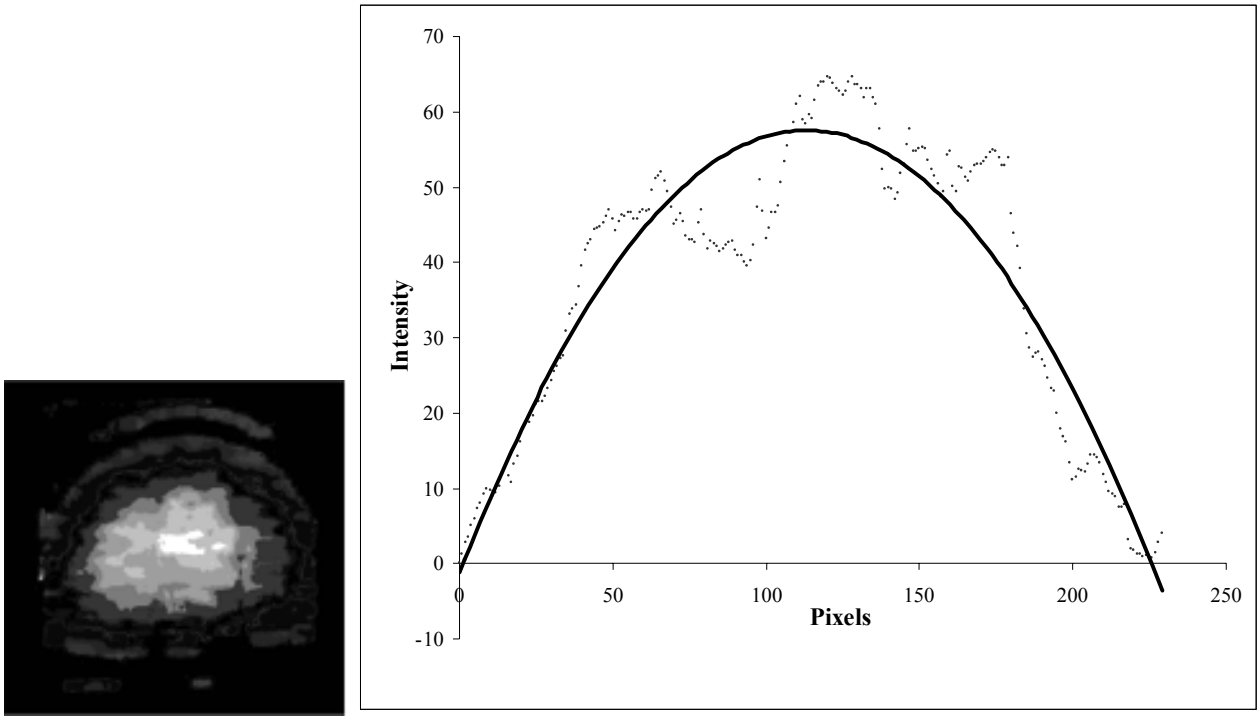

Figure 5. (Left) Doppler signal from 0.8 mm (inner diameter) capillary tube obtained using a commercial Thorlabs OCT system. (Right) Plot of line profile drawn across Doppler image using ImageJ software (ImageJ 1.44f) and the expected parabolic flow profile for laminar flow with a mean velocity of 1.97 mm s-^{1}.

The chosen flow rate was initialised in the capillary tube and a reference frame was noted when flow was established in sample beam **A**. This frame was compared against all subsequent frames of sample arm **B**; i.e. before flow was established in **B**, when the fluid initially encounters the beam (**B**) and when the flow has been established for a large number of **B** frames.

A video of the interference signal was recorded, alternating from one sample beam to the next with each frame. This allowed ease of extraction of the two video frame datasets; all odd frames corresponded to all data related to sample arm **A** (or **B**, depending on the starting point of rotation) and vice versa for all the even frames.

4. RESULTS

The video frames of flow outputted via the CCD camera were extracted using in-house video frame extraction software (Matlab, R2007b).

The processing algorithm as outlined by Xi *et al.*[23] and Tumlinson *et al.*[24] was implemented:

- All frames were converted from RGB to grayscale initially. The spectra acquired were subtracted from the background for direct current removal via reference subtraction;
- Spectral data are nonlinear in *k*-space and therefore must be resampled[25]. This produces a spectrum linear in *k* prior to taking the Fourier transform. The spectrum is linearly interpolated in *k*-space; this is performed using the calibration dispersion mismatch removal technique as outlined by Ding *et al.*[26].
- A Hilbert transform is performed on the resulting data, mapping positive frequency components into the positive-frequency space and negative frequency components into the negative-frequency space of the FFT result, so that the full range frequency space utilised for imaging[27]. Finally, Fourier transformations were obtained of the respective averaged sample frames to obtain A-scan intensity profiles.

Having obtained intensity profiles for every frame, the cross-correlation technique was performed between the reference (**A)** frame and all subsequent **B** (odd or even) frames of the original video. The result of this cross-correlation will be maximised when a similar temporal variation in the light intensity signal as at **A** is detected at **B**.

As it is the flow region within the capillary tube which is of interest, it was necessary to determine whether or not the region of flow was being penetrated by the SLD beams. If this was not the case, no temporal variation in the signal would be observed and if cross-correlation was performed between the two sample arms a high value of correlation would exist (as if it were bulk static tissue in biological terms).

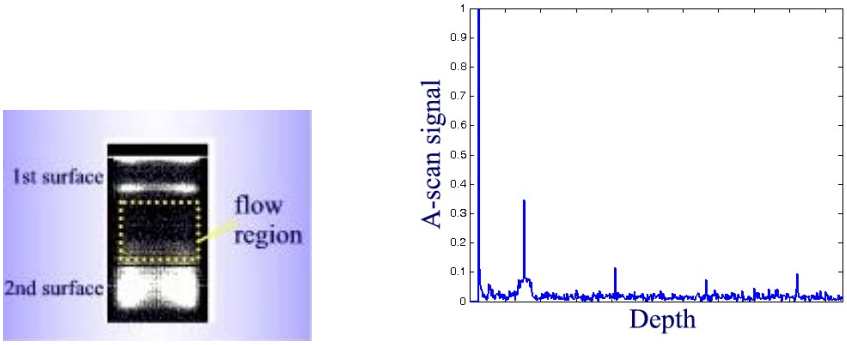

Figure 6. (Left) Post-Fourier transformation image of capillary; center region indicates the area of flow. (Right) Rendered A-scan of capillary.

The above image reveals both the top and bottom surfaces of the capillary, in addition to the flow region situated in between. The maximum penetration depth of an OCT system is derived by the following expression[28]:

$$z_{\max} = \frac{1}{4\eta}\frac{\lambda_0^2}{\Delta\lambda}N \tag{10}$$

where η is the average refractive index of the sample under study (for glass $\eta = 1.5$), N is the number of detector array elements ($N = 1024$), λ_0 and $\Delta\lambda$ are the central wavelength and bandwidth of the chosen light source respectively, as previously described. Using the above expression, the maximum penetration depth of this system was 2.253 mm (in glass) and as the capillary tube falls within this depth, the region of flow is accessed as evident in Fig. 6.

4.1 Cross-correlation of flow signals

The cross-correlation between the reference sample **A** and all subsequent sample **B** frames was performed using Matlab (R2007b). A plot was obtained of the maximum value of correlation over each frame and this was plotted versus the frame identifier (see Fig. 7).

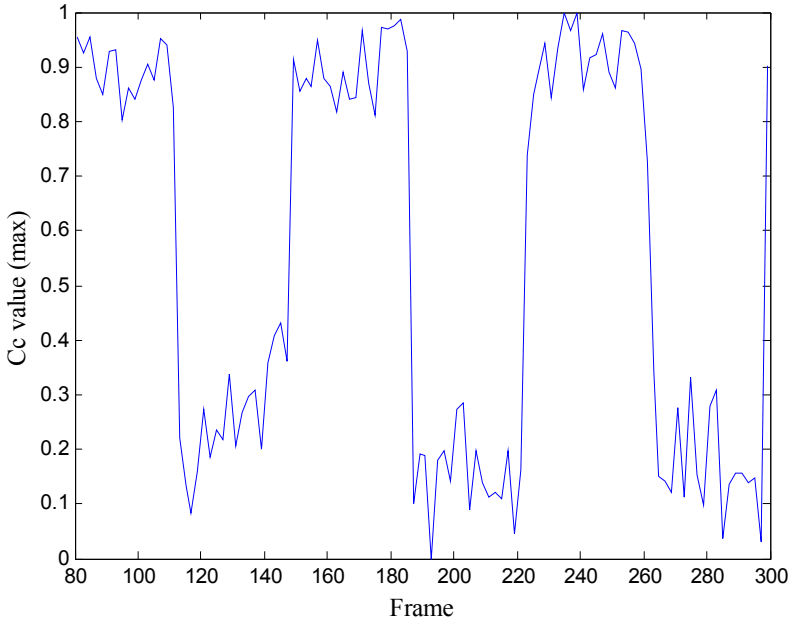

Figure 7. Results of cross-correlation between reference frame (sample arm **A**) and all subsequent (sample arm **B**) sample frames. The highest value of correlation was found to be at frame 239 (arm **B**).

As can be seen from the above plot, a maximum value of correlation was determined at frame 239; the reference frame was chosen to be frame 80. This reference frame was deduced from the observation that flow was definitely established in sample beam **A** and not **B** at that point in time (frame) in the video.

4.2 Velocity computation

As previously mentioned, a laminar flow rate of 0.075 ml/min was chosen. This flow rate corresponds to a volume flow rate (Q) of $1.25\text{x}10^{-9}$ m^3 s^{-1}. The linear flow rate within the capillary tube is calculated via,

$$Q = \frac{dV}{dt} = A.v \tag{11}$$

where A is the cross-sectional area of the capillary and v is the linear velocity within the tube. Using the above expression, the linear velocity for the laminar flow rate applied by the syringe pump is 2.487 mm s^{-1}.

The time between successive frames in the chosen video was 0.033 s. The frame difference between the reference frame (frame 80) and the frame which revealed the maximal value of correlation (frame 239) is 159 frames. This implies that the time lag between the reference frame 80 and frame 235 (i.e. the correlation maximum) is the product of the frame difference and the time difference between successive frames; this time lag ($\Delta\tau$) was determined to be 5.3 s. The spatial separation between the two sample beams impinging on the capillary surface was δ = 0.015 m. Applying these values to the theoretical formulation outlined in §2.2, a value for the velocity obtained within the tube was 2.83 mm s^{-1}; this reveals a 13.79% difference between the experimentally obtained and theoretical laminar flow velocity value.

5. DISCUSSION & FUTURE WORK

The large separation between the sample beam arms (as quoted previously) was necessary due to the design constraints of the focusing lens casing and the available apparatus. Despite this limitation, an appreciable estimation of velocity was obtained, especially when compared with a similar technique using the cross-correlation method with beam separations reported on the scale of tens of microns[29]. Although the velocity value computed resulted in a percentage error of >10%, the previous section revealed that the technique will work, even when the two sample beams are separated on a macro scale (i.e. cm range) if compared to the minute distances (such as the capillary diameter or even source coherence length) also present. The periodicity of the plot of cross-correlation (as featured in Fig. 7) may be attributed to the rotational speed of the scanning mirror delivering the sample arm signals to the spectrograph. The application of an external trigger will be investigated which may compensate for this phenomenon.

The construction of a more robust system setup will be prioritised in the future, especially with regard to the dual beam separation distance. Presently, there is uncertainty with regard to the decorrelation time of the movement of a known volume a certain distance. A computational study is anticipated in the future, investigating how far apart the sample beams have to be for optimised velocity quantification. Use of a single common stationary reference arm for both sample beams may be realised, as it would potentially provide improved system stability for phase-sensitive measurements[16]; in addition, the system would be easier to align.

As the sample reference **A** described in the experiment was obtained purely by means of observation, the prospect of the inclusion of an automated sample reference capture seems probable. This automation would be necessary if the direction of flow was unknown *a priori* (as it is in most cases) and would imply the technique may be used in studies of flow directionality within vessels. Previous work[29] has also shown cross-correlation techniques capable of velocity estimation irrespective of angle. This will also be a topic of forthcoming work.

The described experiment used a flow rate which was laminar or streamline. In laminar flow, the motion of the particles of fluid is very orderly with all particles moving in straight lines parallel to the capillary walls. Turbulent flow within capillaries, however, occurs at higher velocities where small packets of fluid particles (eddies) form leading to lateral mixing. It has not been shown whether this technique would be suitable for velocity quantification applications wherein the flow is not laminar. Applying this velocity measurement technique capable of complex applications will be a topic of future research.

6. CONCLUSIONS

The present study illustrates the potential of using an in-house Spectral domain OCT (SdOCT) system with dual beam configuration for velocity estimation by simultaneously measuring ‘on the fly’ two points a known distance apart. The temporal variations in light intensity were then subjected to computational cross-correlation analysis to determine the transit time, thereby yielding real-time velocity values of flow. In general, the results obtained indicate a tentative first step in developing a robust tool of velocity quantification. Many chronic illnesses manifest in the vascular bed[30]; this area will serve as an ideal starting point to assess both the characteristics of the system as well as its applicability as a clinical tool.

ACKNOWLEDGEMENTS

This research was funded by the Irish Research Council for Science, Engineering and Technology (IRCSET) and is supported by NBIP Ireland funded under the Higher Education Authority PRTLI Cycle 4, co-funded by the Irish Government and the European Union – *Investing in your future*.

REFERENCES

[1] Guiducci, S., Giacomelli, R., and Cerinic, M. M., "Vascular complications of scleroderma," Autoimmunity Reviews 6(8), 520-523 (2007).

[2] Hahn, M.*, et al.*, "Local cold exposure test with a new arterial photoplethysmographic sensor in healthy controls and patients with secondary Raynaud's phenomenon," Microvascular Research 57(2), 187-198 (1999).

[3] Vaz, J. L. P.*, et al.*, "Nailfold videocapillaroscopy in primary antiphospholipid syndrome (PAPS)," Rheumatology 43(8), 1025-1027 (2004).

[4] Aschwanden, M.*, et al.*, "Rapid improvement of nailfold capillaroscopy after intense immunosuppression for systemic sclerosis and mixed connective tissue disease," Annals of the Rheumatic Diseases 67(7), 1057-1059 (2008).

[5] Perez, M. I. and Kohn, S. R., "Cutaneous Manifestations of Diabetes-Mellitus," Journal of the American Academy of Dermatology 30(4), 519-531 (1994).

[6] Scardina, G. A. and Messina, P., "Microvascular abnormalities in patients with rheumatoid arthritis," Annals of Anatomy-Anatomischer Anzeiger 188(5), 425-429 (2006).

[7] Grassi, W.*, et al.*, "Nailfold Capillary-Permeability in Psoriatic-Arthritis," Scandinavian Journal of Rheumatology 21(5), 226-230 (1992).

[8] Vuchetich, J. P.*, et al.*, "High Nailfold Plexus Visibility in Schizophrenia Is Associated with a Distinct Neuropsychological Profile and Less Ventriculomegaly," Schizophrenia Bulletin 35 253-253 (2009).

[9] Leahy, M. J.*, et al.*, "Biophotonic methods in microcirculation imaging," Medical Laser Application 105–126 (2007).

[10] Drexler, W., "Ultrahigh-resolution optical coherence tomography," Journal of Biomedical Optics 9(1), 47-74 (2004).

[11] Fercher, A. F.*, et al.*, "Measurement of Intraocular Distances by Backscattering Spectral Interferometry," Opt. Commun. 117(1-2), 43-48 (1995).

[12] Leitgeb, R., Hitzenberger, C. K., and Fercher, A. F., "Performance of fourier domain vs. time domain optical coherence tomography," Optics Express 11(8), 889-894 (2003).

[13] Hauser, G. and Lindner, M. W., "'Coherence radar' and 'spectral radar'—New tools for dermatological diagnosis," J. Biomed. Opt. 3 21-31 (1998).

[14] Choma, M. A.*, et al.*, "Sensitivity advantage of swept source and Fourier domain optical coherence tomography," Optics Express 11(18), 2183-2189 (2003).

[15] Baumgartner, A.*, et al.*, "Resolution-improved dual-beam and standard optical coherence tomography: a comparison," Graefes Archive for Clinical and Experimental Ophthalmology 238(5), 385-392 (2000).

[16] Bachmann, A. H.*, et al.*, "Dual beam heterodyne Fourier domain optical coherence tomography," Optics Express 15(15), 9254-9266 (2007).

[17] Iftimia, N. V.*, et al.*, "Dual-beam Fourier domain optical Doppler tomography of zebrafish," Optics Express 16(18), 13624-13636 (2008).

[18] Makita S.*, et al.*, "High-sensitive blood flow imaging of the retina and choroid by using double-beam optical coherence angiography," Proc. of SPIE 7550 (2010).

[19] Larina, I. V.*, et al.*, "Live imaging of blood flow in mammalian embryos using Doppler swept-source optical coherence tomography," J. Biomed. Opt. 13(6), (2008).

[20] Ivanovici, M., Iliut, A.-L., and Florea, D., "Vehicle motion tracking by means of cross-correlation," International Congress Automotive, Environment, and Farm Machinery (2007).

[21] Jonathan, E., "Dual reference arm low-coherence interferometer-based reflectometer for optical coherence tomography (OCT) application," Opt. Commun. 252 (2005).

[22] Walther, J. and Koch, E., "Transverse motion as a source of noise and reduced correlation of the Doppler phase shift in spectral domain OCT," Optics Express 17(22), 19698-19713 (2009).

[23] Xi, P., *et al.*, "Evaluation of spectrometric parameters in spectral-domain optical coherence tomography," Applied Optics 50(3), 366-372 (2011).
[24] Tumlinson, A. R., *et al.*, "Inherent homogenous media dispersion compensation in frequency domain optical coherence tomography by accurate k-sampling," Applied Optics 47(5), 687-693 (2008).
[25] Watanabe, Y., *et al.*, "Real-time processing for full-range Fourier-domain optical-coherence tomography with zero-filling interpolation using multiple graphic processing units," Applied Optics 49(25), 4756-4762 (2010).
[26] Ding, C., *et al.*, "A new spectral calibration method for Fourier domain optical coherence tomography," Opt. Int. J. Light Electron. Opt. 121(11), 965-970 (2009).
[27] Wang, R. K., *et al.*, "Three dimensional optical angiography," Opt. Express 15(7), (2007).
[28] Tomlins, P. H. and Wang, R. K., "Theory, developments and applications of optical coherence tomography," Journal of Physics D-Applied Physics 38(15), 2519-2535 (2005).
[29] Shen, Z. Y., *et al.*, "Transverse flow velocity quantification using optical coherence tomography with correlation," Laser Physics Letters 8(4), 318-323 (2011).
[30] Cutolo, M., Pizzorni, C., and Sulli, A., "Capillaroscopy," Best Practice & Research Clinical Rheumatology 19(3), 437-452 (2005).